

Stability limits of n-nonane calculated from molecular dynamics interface simulations

S. Braun, A. R. Imre, and T. Kraska

Citation: *J. Chem. Phys.* **138**, 244710 (2013); doi: 10.1063/1.4811197

View online: <http://dx.doi.org/10.1063/1.4811197>

View Table of Contents: <http://jcp.aip.org/resource/1/JCPSA6/v138/i24>

Published by the AIP Publishing LLC.

Additional information on J. Chem. Phys.

Journal Homepage: <http://jcp.aip.org/>

Journal Information: http://jcp.aip.org/about/about_the_journal

Top downloads: http://jcp.aip.org/features/most_downloaded

Information for Authors: <http://jcp.aip.org/authors>

ADVERTISEMENT

physicstoday

Comment on any
Physics Today article.

Physics Today / Volume 63 / Issue 7 / July 2012
Previous Article | Next Article

Measured energy in Japan
David von Seggern
(dovseg@seismo.unr.edu) University of Nevada
July 2012, page 10
DIGITAL OBJECT IDENTIFIER
<http://dx.doi.org/10.1063/PT.3.1619>

The article by Thorne Lay and Hiroo Kanamori (10.1063/PT.3.1619) is an excellent review of the relationship between seismic moment and energy release. The authors note that the seismic moment is a measure of the size of the rupture, while that of a 100-megaton explosion is approximately five times as much energy as a 10-megaton nuclear detonation event—a 40-megaton atmospheric event. The 1964 Chilean earthquake had still more energy by a factor of about 3, or 15 times that of a 100-megaton nuclear device. I believe the authors used the relation for seismic energy release rather than total strain energy release. The seismic energy underestimates the total strain energy release by a variable that depends on friction on the fault plane. Accounting for total strain energy release would increase the earthquake energy number by orders of magnitude.

Despite the catastrophic damage potential of nuclear bombs, the forces of nature occasionally unleash much larger energy releases. Although the nuclear bombs are under our control, earthquakes, volcanic eruptions, and extreme weather events are not. However, by judicious preparation and avoidance measures, humans can significantly diminish the damage of natural events.

This article does not have any references.

Comment on this article

By the act of hitting a ball with a bat, one calculates the force energy to deliver the ball to its new location, but one must also take into account that the ball extended its energy to the strike team, which became struck by the ball as its momentum ceased and passed energy to the strike team. Therefore the parameters of the damage extend into the future when the received energy to that pushed upon, later becomes released in a new event. Perhaps calculations of one added that in while another's calculations did not. E.M.C.

Written by Edgar Mocarvill, 14 July 2012 19:59

Stability limits of n-nonane calculated from molecular dynamics interface simulations

S. Braun,¹ A. R. Imre,² and T. Kraska¹

¹Institute for Physical Chemistry, University Cologne, Luxemburger Str. 116, 50939 Köln, Germany

²HAS Centre for Energy Research, H-1525 POB 49, Budapest, Hungary

(Received 8 February 2013; accepted 29 May 2013; published online 28 June 2013)

Based on molecular dynamics simulation of the vapor-liquid interface, the classical thermodynamic spinodal for n-nonane is estimated using an earlier developed method. The choice of n-nonane as investigated molecule originates from the question whether a deviation from the spherical symmetry of a molecule affects the prediction of the stability limit data. As a result, we find that the estimated stability limit data for n-nonane are consistent within the experimental data available for the homologous series of the n-alkanes. It turns out that the slight alignment of the molecules parallel to the interface reported in the literature does not affect the method of transferring interface properties to the bulk phase stability limit. © 2013 AIP Publishing LLC. [<http://dx.doi.org/10.1063/1.4811197>]

I. INTRODUCTION

Besides the stable vapor or liquid states of a fluid also so-called metastable states can exist for a certain time, for example, in an overheated liquid. Although one would believe that serious overheating does not happen often or at least it is difficult to be obtained, this is not the case. There are several fields where strongly metastable liquids generated by overheating or stretching exist, for which the limit of metastability becomes important. Metastable liquids boil or rather decompose very rapidly depending on the degree of metastability which can even be explosive. This process sometimes is referred as steam or vapor explosion or flashing. Sometimes this is a useful process but it may also be a process safety problem.

There are plenty applications where the knowledge of stability limits is essential. For economic reasons, gases are often stored in compressed liquid form at temperatures exceeding their atmospheric boiling temperature. In that case, any leak resulting in a pressure drop transforms the formerly stable liquid into metastable liquid that eventually evaporates. If this happens at a very low level of metastability, the process is like an intensive boiling, without any explosive characteristics. However, if it takes place deeply inside the metastable region, the result is a physical explosion¹ damaging the already damaged container to an even larger extent. To be prepared for the worse case scenario one should be aware of the strongest possible metastability, which can be approximated by or in relation to the so-called spinodal curve. Also pressurized liquids are used as cooling or working medium such as water in power plants. In this context, any loss of coolant would cause local pressure drop in the high temperature liquid, causing metastability and eventually vaporization. For a large and rapid pressure drop, explosion-like flashing happens. Here also for safety reason, the knowledge of the stability limits is important.² Another example where the knowledge of the metastable region and its limits is required is the disruptive combustion of fuels³ when explosion-like vaporization of the droplet of a fuel in a liquid matrix happens

in the metastable region. The vaporization will enhance the burning characteristic of the fuel, i.e., the efficiency will be higher.

Just like oversaturated vapor is used to detect various radiations by forming droplets as in the Wilson-chamber, this is also possible for metastable liquids. The so-called Superheat Drop Detectors, also called Superheat Emulsion Detectors (first constructed by Apfel⁴) are using overheated droplets located in a gel or polymer matrix. When the overheated liquid droplet is hit by radiation, it boils immediately, emitting an easily detectable clicking sound. For well-usable detectors, special liquids required that are overheated at room temperature, but still below the critical temperature. For the design of this equipment, stability curves are also required. While in the last two examples the sudden vaporization was a useful process, in the cases mentioned earlier it was an unwanted and harmful one.

A liquid can be overheated or stretched while a vapor can be overpressurised or undercooled. Obviously metastability should have a limit where the system spontaneously decomposes and forms another phase. Figure 1 shows a schematic representation of various stability limit curves together with the vapor pressure curve in the pressure-temperature (pT) projection. The vapor-liquid stability limit is closely above the vapor pressure curve while the liquid-vapor stability limit can reach very large negative pressure values. Here, we focus on the latter liquid-vapor stability limit which is relevant in liquid phase processes. To see the extend of the metastable regions, one should know that water at ambient pressure superheats from 100 °C up to 300 °C. In this way, water can be metastable in a temperature range twice as wide as its stable liquid region.⁵

The furthest stability curves are called spinodals. They are often also referred to as thermodynamic or mechanical stability limit and marked as thin solid curves in Figure 1. At the spinodal, like at a critical point, the isothermal compressibility or isobaric heat capacity diverge.⁵ When approaching the spinodal at some point the initial liquid phase immediately vaporizes in the whole phase volume by the

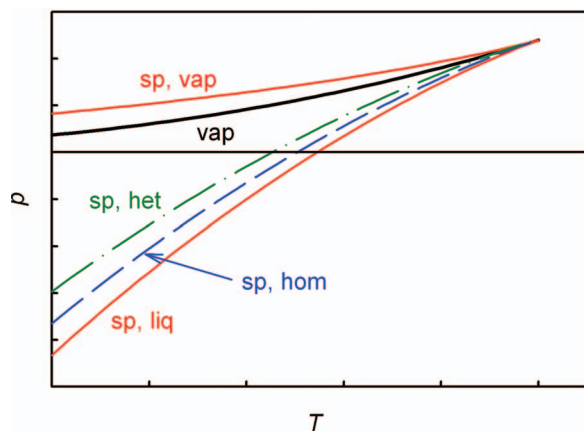


FIG. 1. Schematic representation of the various stability lines. Thick solid curve: vapor pressure curve; thin solid curves: spinodal (sp,vap and sp,liq); dashed curves: homogeneous nucleation limit; and dash-dotted curve: heterogeneous nucleation limit. The horizontal dashed line marks zero pressure. For the sake of better clarity, homogeneous and heterogeneous droplet nucleation curves — located between the sp,vap and vap curves — are not drawn.

so-called spinodal decomposition which differs from the classical nucleation-and-growth mechanism.⁵ In the classical picture, the spinodal is approximated by a curve while fluctuation theory yields a diffuse stripe instead of a sharp curve for this limit.⁶

Another stability limit is the homogeneous nucleation limit which is also called kinetic spinodal. It is drawn as dashed curve in Figure 1 (marked “hom”). At this limit the density fluctuation, which rises when penetrating the metastable region deeper and deeper, is the driving force for the loss of the stability. At a certain point, the density fluctuation is large enough to cross the activation barrier of nucleation leading to decomposition of the system. In this case, the activation barrier of nucleation is smaller than the thermal energy.

The third stability limit is the less well-defined so-called heterogeneous nucleation limit. At this limit, nucleation will be induced by some heterogeneous nuclei like a floating solid contamination or a tiny micro-bubble in a crevice of the container wall. The exact location of this limit depends on the amount of impurity and on the type of impurity with heterogeneous nuclei. In any case, it is always located between the homogeneous nucleation limit and the vapor pressure curve. All the experimental data given as “tensile strength of a liquid” or “limit of attainable superheat of a liquid” are heterogeneous nucleation limits. Only in case of a measurement with very pure substances, the heterogeneous nucleation limit should approach the homogeneous limit. An exception is helium, both helium 3 and helium 4. Since all possible contaminants were frozen out at the temperature at that helium liquefies, always homogeneous nucleation is observed.⁷ Also for helium, one can really reach the spinodal, by changing temperature or pressure rapidly.⁷

Vapor-liquid stability curves follow the same order but they are always at positive pressure since only condensed phases can reach negative pressures.⁸ All these seven stability curves, i.e., the vapor pressure curve, two spinodals, two

homogeneous, and two heterogeneous nucleation limits, terminate at the critical point within the classical picture.

Here we estimate the spinodal of n-nonane from the properties of the vapor-liquid interface using an earlier developed method.⁹ From other investigations, it is known that the chains align slightly parallel to the interface and that the amount of gauche conformations is somewhat higher in the interface.¹⁰ The question here is whether this has an influence on the spinodal estimation.

II. METHOD

The background for the estimation of the spinodal from equilibrium interface data is the observation that the course of the tangential component of the pressure tensor through the interface corresponds to that of the van der Waals loop in the two-phase coexistence region. Early suggestions that the vapor-liquid surface is something like a skin and that the tension of this skin (surface tension) is caused by the difference between the pressure normal $p_N(z)$ and tangential $p_T(z)$ to that skin goes back to the year 1888. For this difference of the pressure components, Fuchs¹¹ derived a function that relates it to the density gradient in the interface:

$$p_N(z) - p_T(z) = q(\rho(z)\rho''(z) - [\rho'(z)]^2). \quad (1)$$

Here $\rho(z)$ is the density profile through the interface and its derivatives with respect to the z coordinate normal to the interface and q is a parameter that has a specific value but it may also be used as adjustable parameter. By suitable integration this expression results into the square gradient theory of van der Waals¹² as well as that of Cahn and Hilliard.¹³

A more rigorous treatment of the relation between the tangential pressure in an interface and the van der Waals loop has been elaborated by Bakker.¹⁴ He argued that the pressure must vary in the interface because the density also varies. He proved by elasticity theory that the normal pressure is actually constant through the interface and has the same value as in the bulk liquid and bulk vapor phases. As a consequence, the normal pressure is the vapor pressure of the system. As discussed earlier,¹⁵ Bakker also related the deviation between the normal and tangential pressure to the surface tension. He called the difference between the pressure components the total deviation to Pascal’s law. Bakker actually makes some suggestions how the tangential pressure may vary with the specific volume (reciprocal density) of the system and compares it with the van der Waals loop. However, he suggested a discontinuous transition from the stable to the metastable region and he also omitted the maximum on the vapor side of the van der Waals loop. On the other hand, he already related the loop of the tangential pressure to labile or metastable states.

With today’s available simulation techniques and computing power, it is possible to determine the tangential pressure profile directly from the molecular interaction of the molecules and employ the profile for the calculation of metastable states from the equilibrium interface and also the stability limit estimation.⁹ For this purpose a simulation system with a stable flat interface is required. This can be

TABLE I. Lennard-Jones parameters for the TraPPE-model.¹⁸

Site	ϵ/k_B [K]	σ [Å]
CH ₄	148	3.73
CH ₃	98	3.75
CH ₂	46	3.95

accomplished by the so-called slab geometry: an equilibrated homogeneous liquid phase in a cubic box is extended by elongation of the box in one direction for which we here chose the z -axis. Periodic boundary conditions stabilize the slab or film leading to an infinitely large film. It should be mentioned that the periodic boundary conditions, in connection with the finite size, limit the wave length of the capillary waves at the interface.¹⁶ However, this effect is not big here as discussed in detail earlier.¹⁵ To avoid the collapse of the film to a sphere it has to have a minimum thickness.¹⁷ A certain thickness is also necessary to obtain bulk liquid phase properties in a significantly thick region in the middle of the film. This and further arguments require a system with at least 1000 molecules, here we simulate system with 8000 molecules using the nine-site TraPPE potential (Transferable Potential for Phase Equilibria) model.¹⁸ This is a united atom model describing n -nonane by nine Lennard-Jones sites each representing a CH₂ or CH₃ group. The Lennard-Jones parameters of these sites are given in Table I. The bond length between the sites is fixed at 0.154 nm, while the bond angle bending is governed by a harmonic potential where the equilibrium angle is set to 114°. The motion of the dihedral angles is described by a torsion potential. This force field has been developed for the accurate simulation of phase equilibrium data. As regular cut-off radius we here use 2.4 nm which is more than six times the largest diameter of the involved sites. This cut-off gives results with by far sufficient accuracy for this investigation. In general, this model has been proven to be accurate for the modeling of the n -alkane series recently.¹⁹

A stable liquid film was obtained by first starting with an equilibration simulation. We start with a simulation box at a density around the corresponding liquid density at given temperature and perform a NVT run lasting 1 ns followed by a short NpT equilibration run to stabilize the system. The simulation box is then elongated three times the box length in the z -coordinate direction and the resulting film is equilibrated in a NVT ensemble at the desired temperature for 2.5 ns which are five runs of 0.5 ns at the same state conditions. To keep the temperature and the pressure constant the Berendsen thermostat ($\tau = 2.0 \times 10^{-3}$) and the Berendsen barostat ($\tau = 5.0 \times 10^{-7}$) are used.²⁰ Full periodic boundary conditions are applied in all steps and the equations of motion are solved by a leap-frog algorithm using an integration step of 1 fs. The center of mass is always set to the center of the simulation box before the interface data are analyzed. This makes sure that a possible fluctuation of the position of the interface does not affect the calculation of the interface properties. For the analysis of the simulation data for the calculation of the pressure tensor, we employ the method of Irving and Kirkwood.²¹

As discussed earlier,²² it is more suitable than the Harasima method.²³

First we have started equilibration simulations, which can typically take 1 ns simulation time. Then simulations for the analysis of the interface properties have been run for typically 2.5 ns. The data for the density and the pressure components obtained from the simulation as function of the z -coordinate being perpendicular to the interface are used to fit the parameters of suitable functions. Here we use a hyperbolic tangens (tanh) based function. Alternatively one may use an error function which is more suitable for modeling fluctuations by means of capillary waves; however, the tanh functions are as good for the analysis required here.^{9,15} For the density profile, we employ

$$\rho(z) = 0.5(\rho_l + \rho_v) - 0.5(\rho_l - \rho_v) \tanh\left(\frac{2(z-l)}{d}\right). \quad (2)$$

To obtain a suitable function for fitting the tangential pressure profile, we apply the equation of Fuchs¹¹

$$p_N(z) - p_T(z) = q(\rho(z)\rho''(z) - [\rho'(z)]^2) \quad (3)$$

as transformation of the density profile yielding a fit function for the tangential pressure profile:⁹

$$p_{NT}(z) = \text{sech}^2(Z)[(a-b)(1 + \tanh^2(Z)) - 2(a+b)\tanh(Z)]. \quad (4)$$

Here Z is given by $Z = 2(z-h)/d$. From the fit of the tangential pressure, the spinodal is determined by calculating the extreme values. The corresponding spinodal pressures at the same temperature can be calculated from the obtained tangential pressure:⁹

$$p = p_N - \frac{3}{2}(p_N - p_T). \quad (5)$$

For a more detailed discussion, see an earlier paper.¹⁵ The z -coordinate at the extreme value of p_T are used to calculate the corresponding density of the spinodal using the fit function of the density profile $\rho(z)$.

Up to now, we have demonstrated the applicability of this method for the Shan-Chen fluid within Lattice-Boltzmann simulations,⁹ for Lennard Jones argon⁹ and carbon dioxide,¹⁵ methanol,²⁴ TIP5P water,²⁵ for helium 3, and helium 4.²⁶ Here we analyze the applicability to molecules with highly anisotropic shape. We address the question, whether the molecular shape influences the predictability of the spinodal from the interface. One might expect that anisotropic properties of the molecules influence the tangential pressure profile and hence the spinodal. Since this is a property of the interface, which is not present in the bulk phase, it is not clear whether for such substances the interface properties can be transformed to the bulk phase stability. As a member of a homologous series, n -nonane is suitable for a systematic analysis. Therefore, in this paper, we calculate the interface properties for n -nonane and compare these with the available stability limit data for the alkanes up to decane using the corresponding states approach.

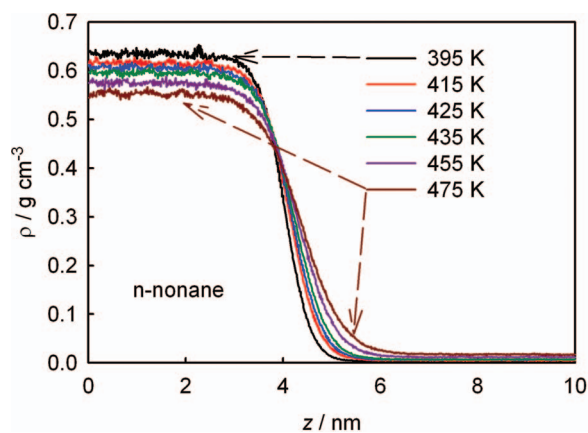


FIG. 2. Density profile through an n-nonane vapor-liquid interface for various temperatures.

III. RESULTS

A. Simulation data

We have performed MD simulations of the vapor-liquid coexistence for six temperatures. In Figures 2 and 3, the density profile and the tangential pressure profiles respectively are shown. Snapshots of corresponding simulation systems are depicted in Figure 4. The graphs represent the average over a 2.5 ns simulation runs at each state conditions. With increasing temperature, the interface widens and the maximum in the plot of $p_N - p_T$ becomes smaller. This corresponds to a shrinking of the area below that curve corresponding to the surface tension. As well known, the surface tension decreases with rising temperature and eventually vanishes at the critical point. The tangential pressure profile exhibits two extreme values a big one on the liquid side of the interface and a small one on the vapor side. These extreme values correspond to the spinodal. From Figures 2 and 3, one can also deduce the error of the simulation data. Here the focus is on the maximum and the minimum of the tangential pressure profile. Hence the uncertainty is related to the uncertainty of the calculation of the maxima and minima. Inspection of Figure 3 suggests a uncertainty of ± 1 MPa. Transferring this to the spinodal diagram

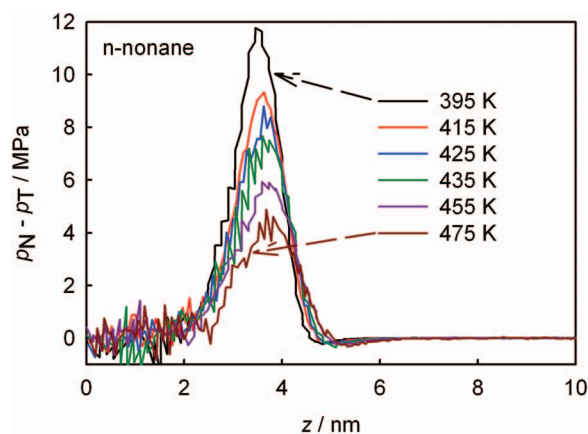


FIG. 3. Profile of tangential pressure (after subtracting the corresponding normal pressure component) through the vapor-liquid interface of n-nonane for different temperatures.



FIG. 4. Snapshots of interface simulation of n-nonane at (a) 395 K and (b) 455 K.

such as Figure 7 gives an error in the order of the size of the plotted symbols.

It is also well known that the choice of a too short cut-off radius has a strong effect on the phase diagram²⁷ and hence also on the surface properties. The surface tension is related to the area under the tangential pressure curve which is in turn related to the extreme values of the tangential pressure profile resulting in the spinodal data. Therefore, one can also expect a strong effect of the choice of the cut-off radius on the spinodal calculation. Figure 5 shows that this is actually the case by comparing a pressure profile for a sufficiently large cut-off of 2.4 nm (6.4σ) and a too short cut-off of 1.4 nm (3.75σ). One can clearly see that a too short cut-off leads to a massive underestimation of the liquid spinodal pressure represented by the maximum. Hence, an accurate estimation of the spinodal by this method requires a sufficiently large cut-off of at least five times the Lennard Jones diameter σ as it is required for the calculation of equilibrium properties. For typical σ -values from 0.34 to 0.4 nm, the cut-off has to be in the order of at least 1.7 to 2 nm.

The resulting spinodal data are plotted in Figure 6 in the density-temperature projection and in Figure 7 in the

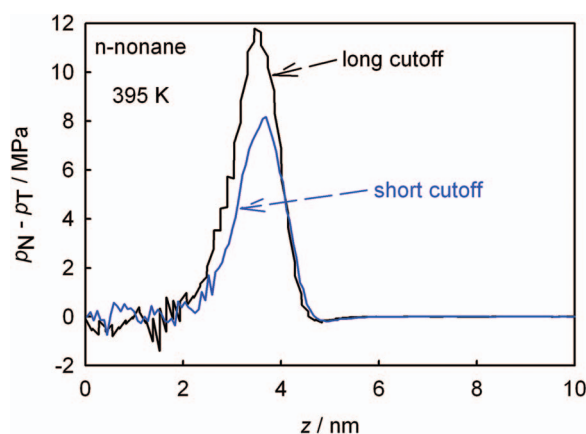


FIG. 5. Effect of the cut-off on the tangential pressure profile through the vapor-liquid interface at 395 K.

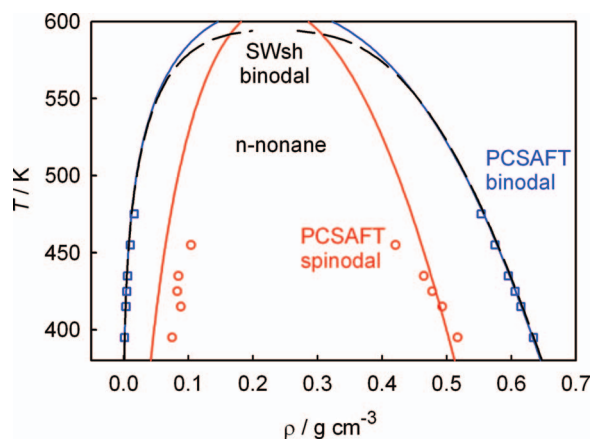


FIG. 6. Temperature-density projection of the vapor-liquid coexistence curve of n-nonane. The symbols are the MD results obtained here. The solid curves are equation of state calculations using the PC-SAFT equation of state. The dashed curve is the binodal calculated with the Span-Wagner reference equation of state.²⁸

temperature-pressure projection. In addition, the equilibrium coexistence data are plotted and compared to several equations of state. The Span-Wagner equation²⁸ is a reference equation which accurately represents the experimental data of stable phase to that it has been fitted. The PC-SAFT equation²⁹ is a molecular-based equation of state suitable for alkanes. The deviation of the PC-SAFT equation in the critical region is a consequence of the classical treatment of the near critical behavior. Obviously the chosen TraPPE force field accurately describes the experimental coexistence data of n-nonane.

B. Equation of state data and experimental data

Attainable superheated states of various alkanes are depicted Figure 8. Although these values are related strictly to the heterogeneous nucleation limit, using very clean sam-

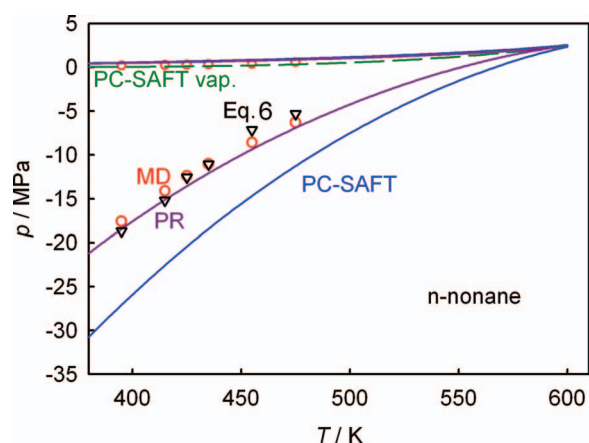


FIG. 7. Pressure-temperature projection of the vapor-pressure curve and the spinodals obtained from simulation (MD, symbols) and the Peng-Robinson (PR)³⁵ as well as the PC-SAFT²⁹ equations of state. The triangles are estimated with Eq. (6) using the simulated surface tension, interface thickness, and vapor pressure. This is a good demonstration for the applicability of Eq. (6) to describe corresponding experimental data. The uncertainty of the simulation data is in the order of the size of the symbols.

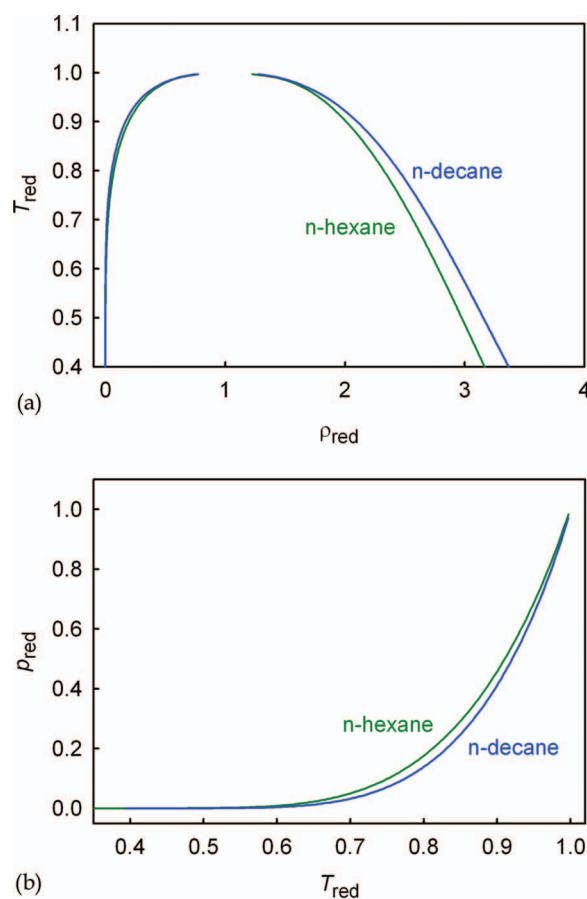


FIG. 8. (a) Binodals of n-hexane and n-decane in density-temperature space. (b) The same in temperature-pressure space. All values are reduced by the corresponding critical values ($p_{red} = p/p_c$, $T_{red} = T/T_c$), obtained from the Wagner-Span reference EoS,²⁸ using the ThermoC program.³⁶

ples one can approach the homogeneous nucleation limit. Also, using very small sample sizes and very fast pressure/temperature changes, the nucleation can be suppressed and the spinodal can be fairly approached although never completely reached. According to the theorem of corresponding states, we scaled these alkanes into the same figure where their vapor pressure curve and hence also their stability limit curves should be more or less the same. To check this validity of this theorem for the n-alkanes, we have plotted the saturation pressures of n-hexane and n-decane in reduced units in Figure 8. Obviously the agreement within the corresponding states principle is not perfect but satisfactory for the analysis here.

In Figure 9 reduced vapor pressure of n-nonane calculated with the Span-Wagner (SW) EoS, the spinodals calculated with the Redlich-Kwong (RK) and a modified van-der-Waals-type equation of state of Quiñones-Cisneros *et al.* (QC-vdW)³⁰ are plotted. The full symbols are experimental data for the n-nonane overheating limits. Some symbols are the available data for n-octane which fall on the same curve within the corresponding state approach. All data are scaled by their critical values. The SW EoS—as a reference equation of state—can describe vapor pressure data accurately, but cannot be applied to metastable states. Therefore, for spinodal calculation other equations of state are used. Especially

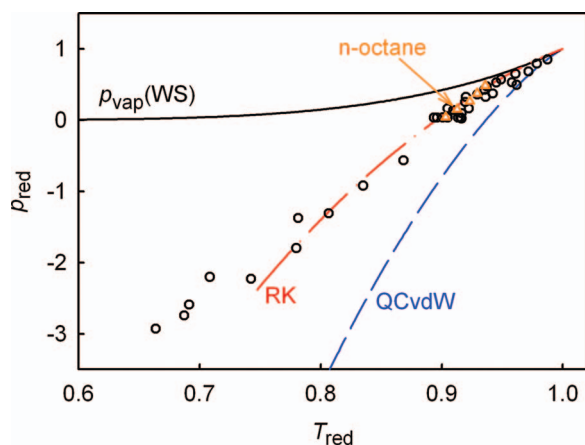


FIG. 9. Reduced vapor pressure of n-nonane obtained from Wagner-Span reference EoS with the calculated spinodals by the original Redlich-Kwong and the modified van-der-Waals by Quiñones-Cisneros³⁰ ($p_{\text{red}} = p/p_c$, $T_{\text{red}} = T/T_c$). Full symbols are measured n-alkane overhear limits, reduced by the corresponding critical properties.^{31,37–43} Since there are no data for n-nonane, data for the closest member of the series n-octane³⁹ are marked by triangles.

the QC-vdW equation is suitable because it very accurately reproduces the vapor pressure and can also be extended into the metastable region. The spinodal calculated from the RK equation is plotted because it is known to describe the overheating limit quite well as it was already discussed by Abbasi and Abbasi for atmospheric pressure in various liquids³¹ and seems to be valid in a wider pressure range too. This agreement—at least with the obtained accuracy—is questionable because the spinodal is the mean field stability limit, while the overheating limit is much closer to the homogeneous nucleation limit and should be above (i.e., at slightly higher pressures) that of the spinodal. So the estimation by the RK equation of state is rather an empirical thumb rule than a reliable prediction.

We have also tested the equation proposed earlier for the calculation of the spinodal pressure from experimental data using the simulation data obtained here. For this analysis, we employed the data for the interface thickness and surface tension both obtained from the simulation and calculated the liquid spinodal pressure according to Eq. (6)⁹ which can also be used for the estimation of the liquid spinodal from equilibrium experimental data only²²

$$p_{\text{sp,liq}} = p_{\text{vap}} - c \frac{\gamma}{d} \quad (6)$$

with $c = 3/2$. Equation (6) fulfills the limiting behavior at the critical point with respect to the values of the properties. As the surface tension approaches zero at the critical point and the interface thickness diverges, the second term vanishes when the critical point is approached. As a consequence, the vapor pressure and the liquid spinodal pressure become identical namely equal to the critical pressure which is consistent with the classical mean field picture of the critical point. It should be noted that the properties in Eq. (6) are also size dependent^{16,32–34} which is here within the mean field approximation and not relevant. It is however not expected that

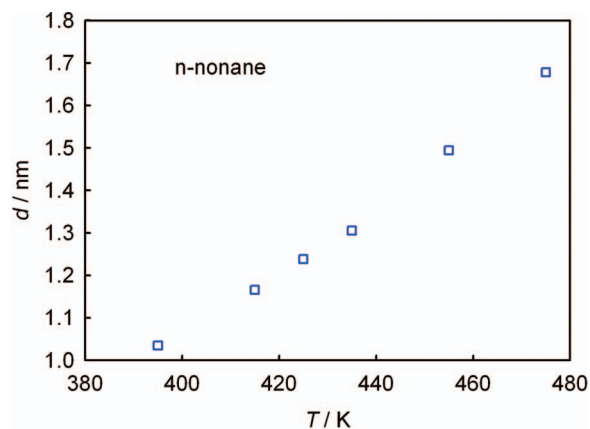


FIG. 10. Interface thickness for n-nonane at different temperatures obtained in MD simulations here.

Eq. (6) fulfills the critical scaling behavior since we found it not accurate in the critical region.¹⁵ With $d \propto |T - T_c|^{-\nu}$, $\gamma \propto |T - T_c|^\mu$, and $|p_{\text{sp}}(T) - p_{\text{vap}}(T)| \propto |T - T_c|^\omega$ in the limit of the critical point, the condition $\omega = \mu + \nu$ should hold according to Eq. (6). In the classical case, the values of the exponents are $\mu = 1.5$ and $\nu = 0.5$ yielding $\omega = 2$. However, numerical analysis using the van der Waals equation of state gives $\omega = 1.6788$. We attribute this difference to the fact that we have omitted the vapor phase peak of p_T that contributes to the calculation of the surface tension. Omitting the vapor phase peak is the result of the simplification to have a handy equation for estimating the spinodal pressure. Hence Eq. (6) is not meant to be an accurate equation in the sense that it fulfills the critical scaling behavior.¹⁵

The simulation data for the interface thickness are plotted in Figure 10 and the surface tension data are compared to experimental data in Figure 11. While there are no experimental data for the interface thickness available for n-nonane, one can clearly see the very good agreement between experiment and simulation for the surface tension. The resulting liquid spinodal data are added in Figure 6 as triangles. Obviously, these data are in very good agreement to the liquid spinodal data obtained from the extreme value in p_T confirming the applicability of Eq. (6).

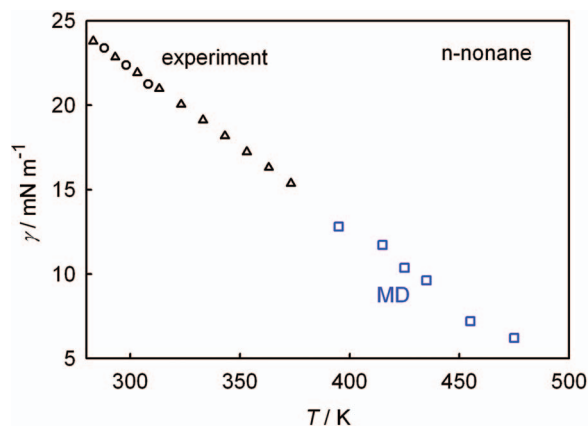


FIG. 11. Surface tension of n-nonane at different temperatures.

IV. DISCUSSION

In this investigation, we have addressed the question whether interface properties can be used for the bulk phase stability for anisotropic molecules. While one can easily be convinced that this is the case for spherical particles such as argon atoms,⁹ it may be questioned for anisotropic molecules. The systems investigated up to now show that at least for small anisotropic molecules such as carbon dioxide¹⁵ (non-spherical and quadrupole), methanol²⁴ (non-spherical and dipole), and also n-nonane, the transformation from the interface to the bulk phase stability yields good estimates for the stability limits. The anisotropic shape of n-nonane apparently does not affect the relation between bulk and interface properties. A possible reason might be that there is no big difference in the molecular orientation and structure in the interface and in the bulk phase observable.¹⁰ One may speculate whether a molecule that is differently oriented in the interface and in the bulk phase may give less accurate estimates for the stability limits but the anisotropic shape of n-nonane is apparently not sufficient for that.

ACKNOWLEDGMENTS

S.B. and T.K. gratefully acknowledge the partial support by Twister B.V. A.R.I. gratefully acknowledge the support of the Humboldt foundation for a three-month stay at the University of Cologne.

¹T. Abbasi and S. A. Abbasi, *J. Hazard. Mater.* **141**, 489 (2007).

²R. Thiéry and L. Mercury, *J. Solution Chem.* **38**, 893 (2009).

³J. C. Lasheras, A. C. Fernandez-Pello, and F. L. Dryer, *Combust. Sci. Technol.* **22**, 195 (1980).

⁴R. E. Apfel, *Nucl. Instrum. Methods* **162**, 603 (1979).

⁵P. G. Debenedetti, *Metastable Liquids: Concepts and Principles* (Princeton University Press, Princeton, NJ, 1996).

⁶K. Binder, *Rep. Prog. Phys.* **50**, 783 (1987).

⁷*Liquid Under Negative Pressure*, NATO Science Series, edited by A. R. Imre, H. J. Maris, and P. R. Williams (Kluwer, 2002).

⁸A. Imre, K. Martínás, and L. P. N. Rebelo, *J. Non-Equil. Thermodyn.* **23**, 351 (1998).

⁹A. R. Imre, G. Mayer, G. Hazi, R. Rozas, and T. Kraska, *J. Chem. Phys.* **128**, 114708 (2008).

¹⁰J. G. Harris, *J. Phys. Chem.* **96**, 5077 (1992).

¹¹K. Fuchs, *Exner's Repertorium Phys.* (München) **24**, 141 (1888), <http://archive.org/stream/repertoriumderp02exnegooq/page/n15/mode/2up>.

¹²J. D. van der Waals, *Z. Phys. Chem.* **13**, 657 (1894) [J. S. Rowlinson, *J. Stat. Phys.* **20**, 197 (1979)].

¹³J. W. Cahn and J. E. Hilliard, *J. Chem. Phys.* **28**, 258 (1958).

¹⁴G. Bakker, *Kapillarität und Oberflächenspannung, Handbuch der Experimentalphysik, Band 6* (Akad. Verlagsges., Leipzig, 1928).

¹⁵T. Kraska, F. Römer, and A. R. Imre, *J. Phys. Chem. B* **113**, 4688 (2009).

¹⁶K. Binder and M. Müller, *Int. J. Mod. Phys. C* **11**, 1093 (2000).

¹⁷S. Werth, S. V. Lishchuk, M. Horsch, and H. Hasse, *Physica A* **392**, 2359 (2013).

¹⁸M. G. Martin and J. I. Siepmann, *J. Phys. Chem. B* **102**, 2569 (1998).

¹⁹E. A. Müller and A. Mejía, *J. Phys. Chem. B* **115**, 12822–12834 (2011).

²⁰H. J. C. Berendsen, J. P. M. Postma, W. F. van Gunsteren, A. DiNola, and J. R. Haak, *J. Chem. Phys.* **81**, 3684 (1984).

²¹J. H. Irving and J. G. Kirkwood, *J. Chem. Phys.* **18**, 817 (1950).

²²A. R. Imre and T. Kraska, *Fluid Phase Equilib.* **284**, 31 (2009).

²³A. Harasima, *Adv. Chem. Phys.* **1**, 203–237 (1957).

²⁴F. Römer, B. Fischer, and T. Kraska, *Soft Mater.* **10**, 130 (2012).

²⁵A. R. Imre, G. Hazi, and T. Kraska, in *NATO Science Series: Metastable Systems Under Pressure*, edited by S. J. Rzoska, A. Drozd-Rzoska, and V. Mazur (Springer, 2009), p. 271.

²⁶A. R. Imre and T. Kraska, *Physica B* **403**, 3663 (2008).

²⁷B. Smit, *J. Chem. Phys.* **96**, 8639 (1992).

²⁸R. Span and W. Wagner, *Int. J. Thermophys.* **24**, 1–39, 41–109, 111–162 (2003).

²⁹J. Gross and G. Sadowski, *Ind. Eng. Chem. Res.* **40**, 1244 (2001).

³⁰S. Quiñones-Cisneros, U. K. Deiters, R. Rozas, and T. Kraska, *J. Phys. Chem. B* **113**, 3504 (2009).

³¹T. Abbasi and S. A. Abbasi, *J. Loss Prev. Process Ind.* **20**, 165 (2007).

³²B. Widom, *J. Chem. Phys.* **43**, 3892 (1965).

³³J. D. Weeks, *J. Chem. Phys.* **67**, 3106 (1977).

³⁴K. Binder, C. Billotet, and P. Mirolid, *Z. Phys. B* **30**, 183 (1978).

³⁵D.-Y. Peng and D. P. Robinson, *Ind. Eng. Chem. Fundam.* **15**, 59 (1976).

³⁶U. K. Deiters, ThermoC, a modular program package for calculating thermodynamic data, 2013, see <http://thermoc.uni-koeln.de/thermoc/index.html>.

³⁷Ho-Young Kwak and Si-Doek Oh, *J. Colloid Interface Sci.* **278**, 436 (2004).

³⁸J. R. Patrick-Yeboah and R. C. Reid, *Ind. Eng. Chem. Fundam.* **20**, 315 (1981).

³⁹C. T. Avedisian, *J. Phys. Chem. Ref. Data* **14**, 695 (1985).

⁴⁰S. Punnathanam and D. S. Corti, *J. Chem. Phys.* **120**, 11658 (2004).

⁴¹J. L. Katz, C. H. Hung, and M. Krasnopoler, in *Atmospheric Aerosols and Nucleation, Lecture Notes in Physics* (Springer, Berlin, 1988), Vol. 309, pp. 356–359.

⁴²J. G. Eberhart and H. C. Schnyders, *J. Phys. Chem.* **77**, 2730 (1973).

⁴³V. E. Vinogradov and P. A. Pavlov, in *Liquid Under Negative Pressure*, edited by A. R. Imre, H. J. Maris, and P. R. Williams, NATO Science Series (Kluwer, 2002), p. 13.